ACCOUNTS of chemical research

pubs.acs.org/accounts Article

Scaffold-Based Functional Models of [Fe]-Hydrogenase (Hmd): Building the Bridge between Biological Structure and Molecular Function

Spencer A. Kerns and Michael J. Rose*

Cite This: *Acc. Chem. Res.* 2020, 53, 1637−1647 Read Online

ACCESS | Metrics & More | Article Recommendations | Supporting Information

CONSPECTUS: The well-known dinuclear [FeFe] and [NiFe] hydrogenase enzymes are redox-based proton reduction and H_2 oxidation catalysts. In comparison, the structural and functional aspects of the *mononuclear* nonredox hydrogenase, known as [Fe]-hydrogenase or Hmd, have been less explored because of the relatively recent crystallographic elucidation of the enzyme active site. Additionally, the synthetic challenges posed by the highly substituted and asymmetric coordination environment of the iron guanylylpyridinol (FeGP) cofactor have hampered functional biomimetic modeling studies to a large extent. The active site contains an octahedral low-spin Fe(II) center with the following coordination motifs: a bidentate acyl−pyridone moiety (C,N) and cysteinyl-S in a facial arrangement; two cis carbonyl ligands; and a H_2O/H_2 binding site. In [Fe]-hydrogenase, heterolytic H_2 activation putatively by the pendant pyridone/pyridonate-O base serving as a proton acceptor. Following H_2 cleavage, an intermediate Fe−H species is thought to stereoselectively transfer a hydride to the substrate methenyl-H_4MPT$^+$, thus forming methylene-H_4MPT. In the past decade, chemists, inspired by the elegant organometallic chemistry inherent to the FeGP cofactor, have synthesized a number of faithful structural models. However, functional systems are still relatively limited and often rely on abiological ligands or metal centers that obfuscate a direct correlation to nature's design.

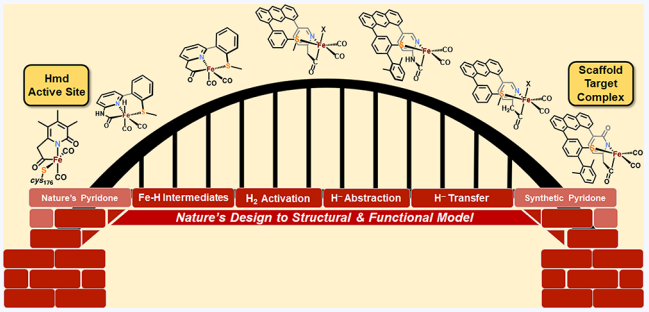

Our group has developed a bioinspired suite of synthetic analogues of Hmd to better understand the effects of structure on the stability and functionality of the Hmd active site, with a special emphasis on using a scaffold-based ligand design. This systematic approach has contributed to a deeper understanding of the unique ligand array of [Fe]-hydrogenase in nature and has ultimately resulted in the first functional synthetic models without the aid of abiological ligands. This Account reviews the reactivity of the functional anthracene-scaffolded synthetic models developed by our group in the context of current mechanistic understanding drawn from both protein crystallography and computational studies. Furthermore, we introduce a novel thermodynamic framework to place the reactivity of our model systems in context and provide an outlook on the future study of [Fe]-hydrogenase synthetic models through both a structural and functional lens.

INTRODUCTION

The dinuclear and mononuclear hydrogenase enzymes catalyze key processes in the energy metabolism of microorganisms through the utilization and generation of dihydrogen (H_2).[1] In nature, the primary roles of the dinuclear [FeFe] and [NiFe] hydrogenases are proton reduction and oxidation of H_2, respectively. These enzymes, in concert with nearby FeS clusters, couple the generation of electrons from H_2 with the reduction of external electron carriers (or vice versa) in various metabolic processes. In contrast, the mononuclear [Fe]-hydrogenase (Hmd) catalyzes the *nonredox* reversible conversion of methenyl-H_4MPT$^+$ to methylene-H_4MPT via a stereoselective hydride transfer reaction.[2−4]

Notably, although the three known classes of hydrogenase enzymes are phylogenetically distinct,[5] convergent evolution has resulted in a shared set of structural characteristics in the form of Fe(II) ligated by carbonyl and thiolato-S ligands. This unique, conserved structural motif is evidently apt for heterolytic H_2 cleavage and has motivated synthetic chemists to design functional catalysts derived from earth-abundant first-row transition metals. Over the last two decades, a number of synthetic models of [FeFe] and [NiFe] hydrogenase have exhibited functional reactivity with H_2—performing H/D exchange, heterolytic cleavage of H_2, and proton reduction—while comparatively fewer complexes have been shown to

Received: May 23, 2020
Published: August 4, 2020

https://dx.doi.org/10.1021/acs.accounts.0c00315
Acc. Chem. Res. 2020, 53, 1637−1647

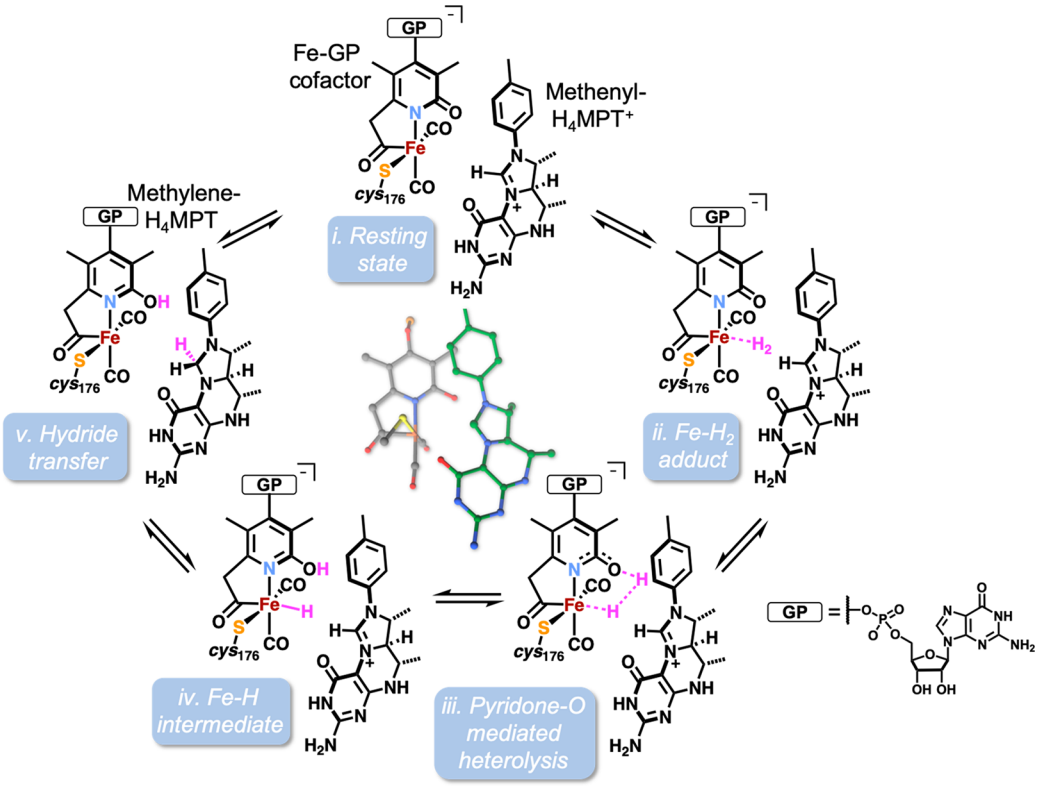

Figure 1. Proposed reactivity cycle of Hmd during catalysis in the closed conformation. The inset shows the truncated molecular structures of the FeGP cofactor in complex with the methenyl-H_4MPT^+ substrate resolved at 1.06 Å.[7]

catalyze the oxidation of H_2.[1,6] In fact, structural model complexes of *mononuclear* [Fe]-hydrogenase have traditionally been catalytically inactive, resulting in little progress in their application to advance mechanistic understanding of enzymatic reactivity with H_2. In [Fe]-hydrogenase, heterolytic H_2 activation is believed to be facilitated by a pendent pyridone/pyridonate-O base that acts as a proton acceptor during catalysis. Following H_2 cleavage, the still-debated intermediate Fe−H species transfers a hydride to the substrate, as depicted in Figure 1.[7]

Several groups have synthesized complexes that reliably mimic structural motifs in [Fe]-hydrogenase, incorporating essential structural aspects such as the organometallic acyl Fe−C bond, a thiolato-S donor, two carbonyl ligands, and even the phosphato substitution of the pyridine moiety (Figure 2).[8−13] Additionally, substitution of various functional groups (e.g., −OH,[14,15] −OMe,[10] or $-NH_2$[16]) at the ortho position of the pyridine has been achieved. However, these models were not reported to react with H_2. In the case of the −OH- and −OMe-substituted complexes, the pK_a values for the conjugate acids (i.e., BH^+) are far too low to reasonably suspect that these pendant groups can serve as bases in the H_2 splitting reaction. Indeed, computational studies have predicted that the pK_a of the Fe(η^2-H_2) species (Figure 1, step *ii*) of the enzyme is roughly 9.[17] In related work, Hu and co-workers reported a diphosphine ligand resembling the azadithiolate ligand of [FeFe] hydrogenase to achieve H_2 activation and aldehyde hydrogenation.[18] Additionally, incorporation of a model compound into the Hmd apo-enzyme enabled 1% activity of the native active site.[19] For this reason, the literature has traditionally asserted the importance of the protein architecture and its conformational changes in the presence of the substrate (methenyl-H_4MPT^+) as crucial to obtain H_2-based reactivity with synthetic models of [Fe]-hydrogenase.

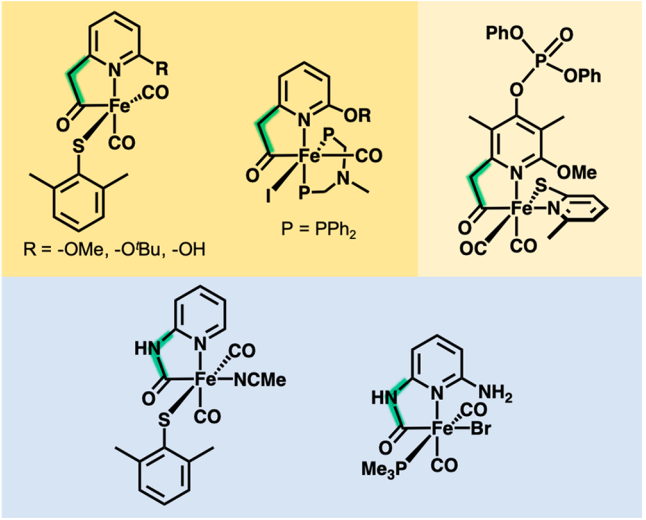

Figure 2. Representative examples of nonscaffolded synthetic model complexes by the Hu (yellow), Song (pale yellow), and Pickett (blue) groups. The acyl (yellow background) or carbamoyl (blue background) functional group of each model complex is outlined in green.

In our research, we have leveraged a "scaffold" format to develop a bioinspired set of synthetic analogues of Hmd in order to better understand the effects of structure on the stability and functionality of the Hmd active site.[20] We have employed three general ligand systems in order to achieve this goal: the scaffold-based *fac*-C,N,S,[21−23] *mer*-C,N,S,[24−26] and *mer*-N,N,S[27,28] donor sets. This systematic approach has

https://dx.doi.org/10.1021/acs.accounts.0c00315
Acc. Chem. Res. 2020, 53, 1637−1647

contributed to understanding the role of the identity and geometry of the unique ligand array of [Fe]-hydrogenase in nature and ultimately resulted in the first functional synthetic models without the aid of abiological ligands. This Account will review the reactivity of the functional anthracene-scaffolded synthetic models in the context of current mechanistic understanding drawn from protein crystallography and computational studies on [Fe]-hydrogenase to provide an outlook on the future study and applications of [Fe]-hydrogenase synthetic models.

MECHANISTIC GUIDANCE FROM COMPUTATIONAL STUDIES

As no reactive intermediates have been experimentally observed during catalysis, the understanding of the Hmd mechanism has been advanced via computational studies. Applying nascent crystal structures, Hall utilized truncated active site models and density functional theory (DFT) methods to investigate the mechanism of Hmd.[29,30] In these studies, the presence of the substrate methenyl-H_4MPT^+ was essential to lowering the barrier involved in heterolytic H_2 cleavage. Hall elucidated two viable pathways to H_2 activation: mediated by either the cysteinyl thiolato-S or the pyridone-O as a proton acceptor. Following H_2 binding and polarization, the substrate methenyl-H_4MPT^+ was demonstrated to ultimately "trigger" cleavage of the H_2 bond. In this work, the rate-limiting step was identified as hydride transfer to the substrate following protonation of the pyridone-O (Figure 1, step *v*). This assignment is consistent with experimental results in which the V_{max} and K_m of Hmd under H_2 and D_2 indicated no kinetic isotope effect (KIE) associated with heterolysis.[31]

Reiher[32] and later Shima[7] performed QM/MM calculations on Hmd to investigate the effects of the protein environment on catalysis. Reiher found that H_2 heterolysis across the pyridone-O (Figure 1, step *iii*) is favored over that across the thiolato-S by 14.3 kcal mol^{-1}. Still, heterolysis mediated by thiolato-S remained exothermic by 4.4 kcal mol^{-1}, indicating that the bound thiolate is a possible proton acceptor, which is consistent with the observable activity (1%) maintained in the H14A Hmd mutant.[3] Furthermore, in the favored pathway, a stable minimum corresponding to an Fe−H species (Figure 1, step *iv*) could not be calculated, suggesting a concerted heterolysis mechanism and direct hydride transfer from H_2 to methenyl-H_4MPT^+; the ternary complex is composed of the iron guanylylpyridinol (FeGP) cofactor, H_2, and methenyl-H_4MPT^+. This observation is consistent with current experimental results that have not shown an electronic change in the Fe center corresponding to a hydride species.[33,34] Most recently, Shima utilized QM/MM calculations to support the role of the pyridone-O in heterolysis and, in contrast, did find that a stable Fe−H species was possible and stabilized by interactions with the substrate. Additionally, these calculations supported H_2 heterolysis (Figure 1, step *iii*) as the rate-limiting step in catalysis, in contrast to the hydride transfer step as proposed by Hall.

DESIGN PRINCIPLES OF AN ANTHRACENE SCAFFOLD FOR Hmd MODEL COMPOUNDS

The prevalence of facial coordination motifs in bioinorganic coordination chemistry has inspired the design of useful synthetic ligands such as tris(2-pyridylmethyl)amine (TPA), 1,4,7-triazacyclononane (TACN), and tris(pyrazolyl)borate (Tp) in modeling histidine-rich environments such as cysteine dioxygenase (CDO)[35] and carbonic anhydrase (CA).[36] However, the active site of [Fe]-hydrogenase presents a unique challenge to the synthesis of model compounds because of (*i*) the highly *asymmetric* first coordination sphere and (*ii*) the highly *functionalized* secondary coordination sphere (especially the pyridone moiety). Our motivating approach to modeling [Fe]-hydrogenase was to develop a ligand featuring a tridentate chelate that enforced facial coordination of the organic C, N, and S donors. We turned to molecular scaffolding, inspired by its utility in both enforcing ordered structural arrangements and imparting stability in past bioinorganic model systems. For example, a trisubstituted benzene scaffold was utilized by Holm for Fe_4S_3 complexes[37] and Agapie for Mn-OEC model compounds,[38] exemplifying a scaffold-based approach to threefold-symmetric metal binding motifs. More recently, the Suess group leveraged this platform to generate site-differentiated Fe−S clusters and the first $[Fe_4S_4]$−alkyl cluster.[39] Additionally, Lippard utilized a substituted triptycene scaffold in modeling the carboxylate-bridged diiron sites of bacterial multicomponent monooxygenase.[40]

Our approach also "builds upon" the symmetric dibenzofuran (DBF) and anthracene scaffolds utilized by the groups of Lu[41,42] and Gelman,[43,44] respectively. Briefly, we have employed a substituted 1,8-anthracene moiety as the scaffold foundation, as utilized in the trans-spanning, para-linked phosphine ligand developed by Gelman. However, we have opted to attach the metal-binding donor "arms" at the meta position with respect to the anthracene scaffold, as exemplified in the DBF-scaffolded complexes of Lu. Critically, this construction allows for substitution on both ortho sites (Scheme 1, green) of the N and S donor atoms, thus enabling

Scheme 1. Chemical Representation of Our Tethered Anthracene Scaffold Approach to Obtain the Asymmetric *fac*-C,N,S Coordination Motif of [Fe]-hydrogenase; Important Ortho Sites for Substitution Are Highlighted in Green

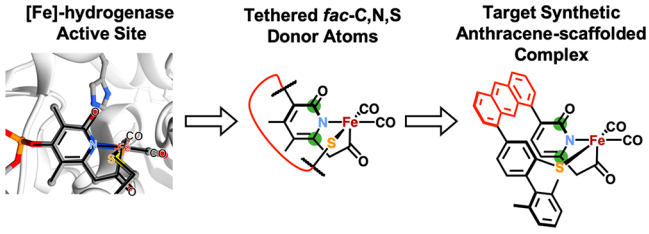

incorporation of the biomimetic methylene acyl Fe−C bond and pyridone moieties of the Hmd active site. A more comprehensive review of each system and a comparison of a wide variety of scaffold bite angles, donor atom distances, and scaffold−aryl torsion angles was previously reported.[45] Utilizing this asymmetrically substituted 1,8-anthracene as a scaffold, we have developed a modular synthetic approach that facilitates access to a variety of highly substituted ligand donor arms.

A BIOMIMETIC REACTIVITY SYSTEM FOR Hmd CATALYSIS

In nature, Hmd catalyzes the heterolytic cleavage of H_2 via metal−ligand cooperation between the Fe center and the

https://dx.doi.org/10.1021/acs.accounts.0c00315
Acc. Chem. Res. 2020, 53, 1637−1647

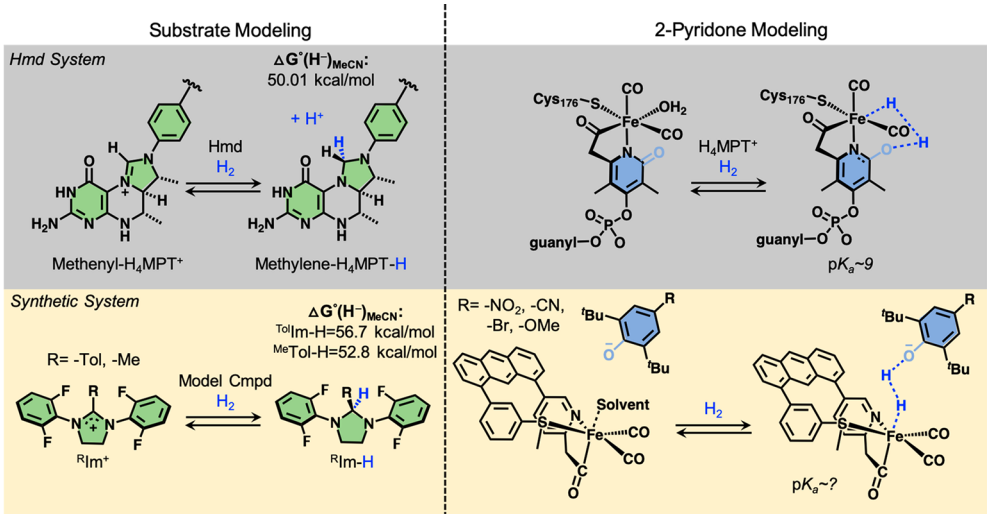

Figure 3. Comparison of components involved in the native reactivity of Hmd (gray) and functional biomimetic synthetic systems (yellow). Structural similarities of methenyl-H_4MPT$^+$ and ^{R}Im$^+$ are highlighted in green, and calculated thermodynamic hydricities[47,48] are presented. Structural similarities of the 2-pyridone moiety and exogenous phenolate base are highlighted in blue, and approximate pK_a values are provided.

pendent pyridone-O atom of the FeGP cofactor; subsequently (or concomitantly in the ternary complex), the hydride is transferred from the Fe center to the substrate methenyl-H_4MPT$^+$. The incorporation of 2-pyridone moieties in stable Fe-containing synthetic models of Hmd has proven to be an exceedingly difficult synthetic challenge. Thus, we sought to apply a bioinspired approach that would enable the study of model compounds with H_2(or D_2) and methenyl-H_4MPT$^+$ model substrates to study the endogenous hydride transfer reaction.

The model substrates 1,3-bis(2,6-difluorophenyl)-2-(4-tolyl)imidazolium (^{Tol}Im$^+$) tetrakis(3,5-bis(trifluoromethyl)-phenyl)borate and 1,3-bis(2,6-difluorophenyl)-2-methylimidazolium (^{Me}Im$^+$) tetrakis(3,5-bis(trifluoromethyl)phenyl)borate were utilized as analogues of the methenyl-H_4MPT$^+$ substrate. Meyer and co-workers initially developed ^{Tol}Im$^+$ as a model substrate for hydride transfer to methenyl-H_4MPT$^+$ from a ruthenium cyclopentadienyl carbonyl compound.[46] As highlighted in Figure 3, ^{Tol}Im$^+$ and ^{Me}Im$^+$ approximate the core imidazolium structure present in methenyl-H_4MPT$^+$. The electron-withdrawing *N*-difluoroaryl substituents improve the hydride-accepting ability and provide an additional NMR spectroscopic handle. Substitution of C-2 additionally affords a handle to modulate the hydricity of the substrate, provided that substrate pyramidalization at C-2 is still accessible and the substituent is not prohibitively bulky. Utilizing the DFT methods of Glusac and co-workers,[47] we calculated the hydricities (calculated in acetonitrile) of ^{Tol}ImH and ^{Me}ImH to be 56.7 and 52.8 kcal/mol, respectively. The analogous value for the biological hydride donor methylene-H_4MPT is 50.01 kcal/mol.[48] These values provide a framework to understand the *relative* hydride donor strengths of organic model substrates and synthesized metal complexes, despite the caveat that such hydride transfer reactions involving first-row transition metals are often incompatible with strongly coordinating solvents like acetonitrile.

Thus far, we have utilized the exogenous base tetraethylammonium 2,6-di-*tert*-butyl-4-methoxyphenolate, (Et_4N)[MeO^{t}Bu$_2$ArO], as a substitute for the intrinsic basic pyridonate-O site of Hmd. Indeed, the anionic phenolate-O of [MeO^{t}Bu$_2$ArO]$^-$ closely approximates the pK_a of the proposed active pyridonate-O invoked in Hmd catalysis. For comparison, [MeO^{t}Bu$_2$ArO]$^-$ is moderately more basic (conjugate acid pK_a(H_2O) ≈ 13)[49,50] than the pyridonate-O of the enzyme active site (conjugate acid pK_a(H_2O) ≈ 11.7).[51] The two *o*-^{t}Bu groups nominally prevent coordination of the metal center by the base, while the *para* substituent provides a means for modulating the strength of the base (and thus an indirect means to study the acidity of the Fe—H_2 adduct).

FUNCTIONAL MODEL COMPLEXES OF [FE]-HYDROGENASE

Modeling the Reverse Reaction (C—H Hydride Abstraction): Scaffold *fac*-C,N,S Thioether

Recently, our group reported the synthesis and reactivity of parent complex **1-Br** (Figure 4), the first example of a C,N,S-derived model system to react with H_2.[21] Model **1-Br** was synthesized from a procedure using $Fe(CO)_4Br_2$ in DCM at −30 °C.[11] Nucleophilic attack of a carbonyl in the metal salt by the amine moiety of the ligand results in the carbamoyl Fe—C bond, which serves as a structural approximation of the

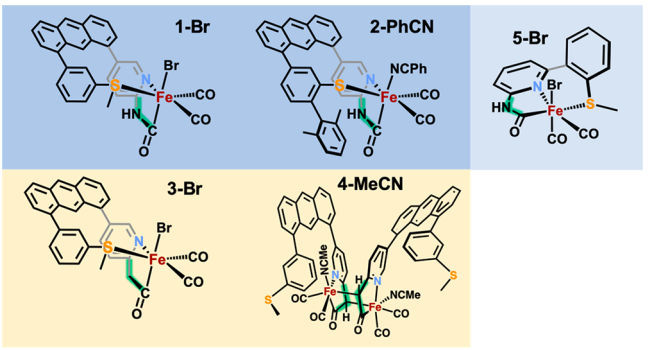

Figure 4. Summary of synthetic complexes discussed in this Account. Complexes containing the carbamoyl functional group are depicted with a blue background, and complexes containing the acyl functional group are depicted with a yellow background. The identity of the variable sixth ligand at the position trans to the organometallic Fe—C bond is specified in the nomenclature.

https://dx.doi.org/10.1021/acs.accounts.0c00315
Acc. Chem. Res. 2020, 53, 1637−1647

native methylene(acyl) ligation.[11] Complex **1-Br** exhibits ν(CO) frequencies at 2031 and 1981 cm^{-1} and a feature at 1661 cm^{-1} corresponding to the carbamoyl C═O bond, as summarized in Table 1.

Table 1. Summary of Infrared ν(CO) Features of Model Compounds Discussed Herein

complex	ν(C≡O) (cm^{-1})	ν(C═O) (cm^{-1})
1-Br	2031, 1981	1661
2-PhCN	2016, 1956	1632
3-Br	2039, 1978	1629
4-MeCN	2021, 1998, 1962, 1943	–
5-Br	2034, 1974	1619
Hmd[a]	2011, 1944	–
FeGP[b]	2029, 1957	1697

[a]Values for Hmd enzyme reported in H_2O at pH 6.0.[52] [b]Values for acetic acid-extracted FeGP cofactor (dried sample).[53]

The starting complex was activated by halide abstraction utilizing Tl(BAr^F_4), resulting in the weakly bound THF solvato species $\mathbf{1}^+$ with an open reactive site. Hydride abstraction from the model substrate ^{Tol}ImH by $\mathbf{1}^+$ was indicated by ^{1}H NMR analysis by complete loss of the methine resonance at 6.12 ppm and generation of $^{Tol}Im^+$ (Figure 5A). However, upon

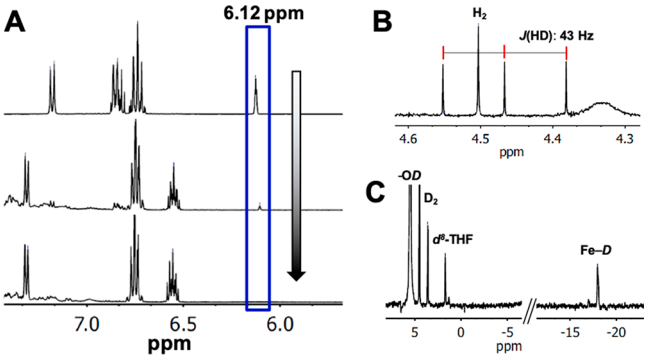

Figure 5. (A) ^{1}H NMR spectrum in THF-d_8 demonstrating hydride abstraction from ^{Tol}ImH by $\mathbf{1}^+$, as outlined in Scheme 2. (B) ^{1}H NMR spectrum demonstrating H/D scrambling activity in the presence of MeO^{t}Bu$_2$ArOD. (C) ^{2}H NMR spectrum demonstrating generation of the Fe−D species.

abstraction no Fe−H species was observable by NMR spectroscopy. Nonetheless, the catalytic nature of this reaction was further confirmed by repeating the experiment with 5 equiv of ^{Tol}ImH and 5 equiv of MeO^{t}Bu$_2$ArOH. Analysis of the headspace gas showed the production of H_2 with consistent multiple turnovers, demonstrating the enzymatic "reverse reaction" (H^+ + [C−H] → H_2 + [C^+]).

The biomimetic forward reaction was investigated through the reactivity of the complex with D_2. Incubation of the activated complex with D_2 resulted in the appearance of a new signal in the ^{2}H NMR spectrum at 7.78 ppm, corresponding to the −NH resonance observed in the ^{1}H NMR spectrum at 7.70 ppm. Furthermore, the broad singlet at 7.70 ppm in the ^{1}H NMR (THF-d_8) spectrum was abolished upon addition of D_2 gas. Inspection of the infrared spectrum showed no discernible difference between $\mathbf{1}^{NH}$ and $\mathbf{1}^{ND}$, confirming the structural integrity of the metal complex following the conversion. H/D scrambling activity by $\mathbf{1}^+$ was observed upon treatment with D_2 and the proton source MeO^{t}Bu$_2$ArOH, as signified by new ^{1}H NMR resonances corresponding to H_2 and HD as a singlet at 4.50 ppm and a triplet at 4.47 ppm (J(HD) = 43 Hz), respectively (Figure 5B). The converse isotopic study (i.e., H_2, MeO^{t}Bu$_2$ArOD) similarly resulted in the observance of newly generated D_2 gas in the ^{2}H NMR spectrum, confirming the H/D scrambling activity of complex $\mathbf{1}^+$ in the presence of a substrate (H^+).

Encouraged by the H_2 activation demonstrated by $\mathbf{1}^+$, the analogous enzymatic "forward" reaction, or hydride transfer to an organic substrate ($^{Tol}Im^+$), was attempted but proved to be unsuccessful. The H/D scrambling activity of $\mathbf{1}^+$ presumably proceeds through an intermediate Fe−H or Fe−D (as depicted in Scheme 2), which was unobserved in the previous reactions.

Scheme 2. Summary of (*i*) Hydride Abstraction from the Model Substrate ^{Tol}ImH Coupled with (*ii*) Hydride Transfer to a Proton Source to Generate H_2 Demonstrated through Intermediate 1-H

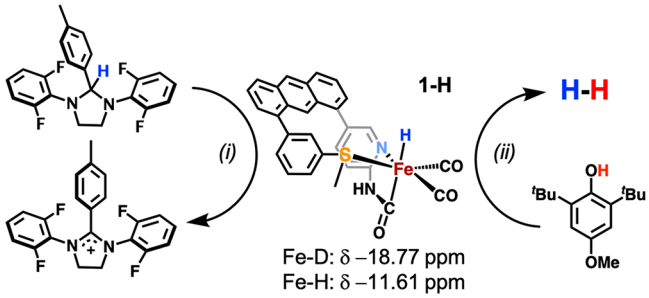

In attempts to prevent H/D crossover and observe the putative intermediates, the aforementioned reactions were performed under deuterium-rich conditions (i.e., D_2, MeO^{t}Bu$_2$ArOD), resulting in a stable Fe−D resonance observed at −17.96 ppm in the ^{2}H NMR spectrum (Figure 5C). This process was demonstrably dependent on the pressure of D_2 present in the reaction mixture, with the conversion to the Fe−D product diminished from 20% at 7 atm D_2 to 2% at 1 atm D_2. The persistent Fe−D species observed contrasts with the fact that no such related intermediate has been observed in the enzyme to date.

Modeling the Forward Reaction (H_2 → Hydride Transfer): Scaffold *fac*-C,N,S Thiolate

Next, we developed a more faithful model of Hmd by incorporation of a thiolato-S donor in place of the thioether moiety utilized in complex **1-Br**.[22] A bulky 2,6-dimethylphenyl group was appended at the ortho position of the thiolato-S donor to prevent the formation of higher-nuclearity metal complexes that often result from bridging thiolates. The thiolate-containing complex **2-PhCN** (Figure 4) exhibits ν(CO) frequencies at 2016, 1956, and 1632 cm^{-1}, which are significantly lower in energy than those of the thioether-containing species and consistent with those of the Hmd enzyme in water (2011 and 1941 cm^{-1}) and other model systems.

Complex **2-PhCN** was isolated as the PhCN solvato-bound species and structurally characterized by X-ray crystallography (Figure 6A), confirming the viability of the anthracene scaffold in generating a tridentate *fac*-C,N,S chelate in a mononuclear thiolate format. The average Fe−C bond distance of the organometallic carbamoyl unit in **2-PhCN** (1.9555 Å) is longer than that observed in Hmd (1.880 Å) but consistent with

https://dx.doi.org/10.1021/acs.accounts.0c00315
Acc. Chem. Res. 2020, 53, 1637−1647

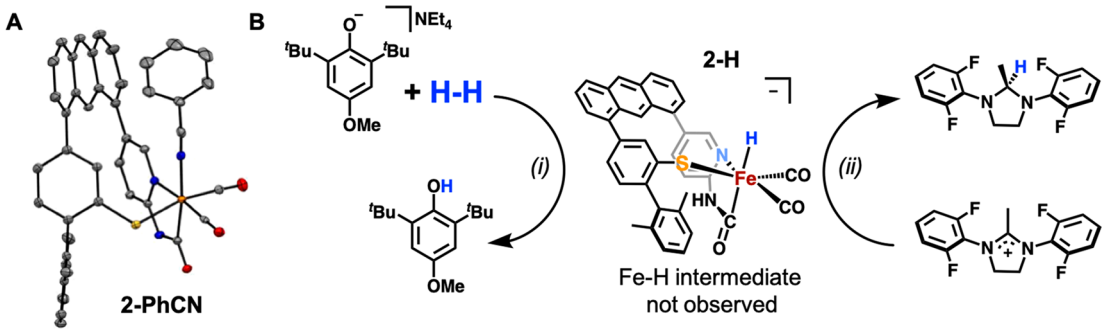

Figure 6. (A) Molecular structure of **2-PhCN** demonstrating the anthracene-scaffolded *fac*-C,N,S three-membered chelate. Atom colors: carbon (gray), nitrogen (blue), oxygen (red), sulfur (yellow), iron (orange). (B) Summary of (*i*) H_2 activation and (*ii*) hydride transfer to the model substrate $^{Mel}Im^+$ demonstrated by the parent complex **2-PhCN**.

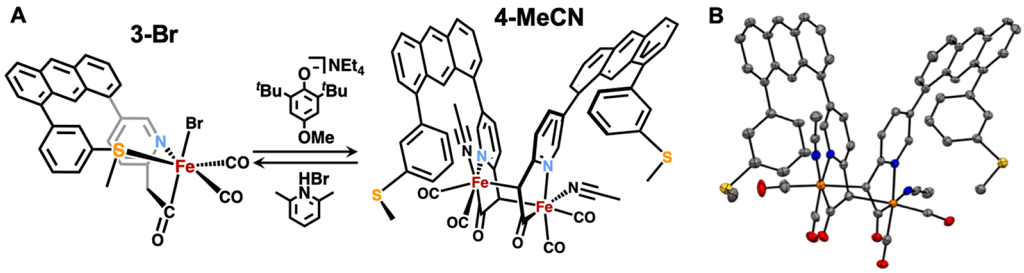

Figure 7. (A) Deprotonation of the methylene protons of **3** to form **4**. (B) Molecular structure of **4**. Atom colors: carbon (gray), nitrogen (blue), oxygen (red), sulfur (yellow), iron (orange).

those in other Hmd model complexes. The coordination of the Fe center by the tridentate anthracene-derived chelate results in significant changes in the angles observed in the complex. Complex **2-PhCN** exhibits a 2° larger C−Fe−S angle (80.14°) in comparison with that observed in Hmd (77.35°), while the N−Fe−S bite angle (93.84°) is nearly 10° wider than that observed in Hmd (84.20°). Furthermore, coordination of the Fe center results in a 9.98 ± 3.07° torsion across the plane of the anthracene scaffold of the ligand, suggesting that an expanded or more flexible scaffold may better accommodate the binding of the Fe center in future model compounds.

The reactivity of complex **2-PhCN** with D_2 was studied to provide insight into the functional role of the cysteine thiolate—the only protein-derived ligand donor. Treatment of complex **2-PhCN** with 7 atm D_2 in CH_2Cl_2 did not result in any new resonances in the ^2H NMR spectrum. This result seems to preclude the role of the cysteinyl sulfur as the favored base in H_2 cleavage and underscores its likely role as a structural anchor in the enzyme during catalysis. Additionally, this result contrasts with the related reaction of D_2 and thioether-bound $\mathbf{1}^+$ where NH → ND exchange was observed.

The viability of **2-PhCN** to activate dihydrogen was then studied in the presence of an exogenous base, $[MeO^tBu_2ArO]^-$. Under 7 atm D_2, a new resonance in the ^2H NMR spectrum was observed at 4.89 ppm, corresponding to MeO^tBu_2ArOD. However, a resonance corresponding to the expected Fe−*D* product was not observed, suggesting a reactive or unstable metal hydride species. The same experiment was repeated in the presence of the model substrates $^{Tol}Im^+$ and $^{Me}Im^+$. Interestingly, hydride transfer to $^{Tol}Im^+$ was not observed despite its greater hydride-accepting ability. However, a new resonance at 5.39 ppm corresponding to the hydride transfer reaction product ^{Me}ImD was observed in concert with proportional growth of the MeO^tBu_2ArOD resonance when $^{Me}Im^+$ was used as the substrate. We presently explain this paradoxical result as a steric incompatibility of the anthracene scaffold and bulky *o*-dimethylphenyl unit of **2-PhCN** with the $^{Tol}Im^+$ substrate, as an argument based on the hydricities of the substrates predicts the opposite result (vide supra, Figure 3).

The aforementioned hydride abstraction reaction from model substrate performed by $\mathbf{1}^+$ was also investigated with **2-PhCN**. However, hydride abstraction by **2-PhCN** did not proceed. This result further exemplified the reaction bias in our model compounds and suggests that a secondary-coordination-sphere interaction may be important in gating bidirectional Hmd reactivity (vide infra, in Extant Challenges in [Fe]-Hydrogenase Synthetic Modeling). Furthermore, an Fe−*D* resonance was never observed by NMR spectroscopy in reactions containing **2-PhCN** and D_2, consistent with both experimental and computational studies performed on the enzyme.

Limitations of the (Acyl)methylene Linkage: Scaffold *fac*-C,N,S and Iron Carbonyl Extrusion

A comparison of past structural models has revealed that little structural difference exists between complexes containing an amide (−NH; carbamoyl) linkage and those containing a methylene ($-CH_2$; acyl) linkage. However, a carbamoyl-containing model complex that was synthesized by the Pickett group binds acetonitrile in the position trans to the Fe−C unit,[11] while a close structural analogue bearing an acyl Fe−C unit prepared by Hu and co-workers does not bind a sixth ligand,[10] suggesting a significant electronic difference between the two closely related organometallic donors. Inspired by this observation, we sought to synthesize an acyl-containing model compound analogous to **1-Br** to observe a possible functional difference between these two common features prevalent in Hmd model compounds.

https://dx.doi.org/10.1021/acs.accounts.0c00315
Acc. Chem. Res. 2020, 53, 1637−1647

We prepared the acyl-containing compound **3-Br** (Figure 4) and first attempted experiments parallel to those performed with **1-Br**.[23] However, the reaction of **3-Br** activated with $Tl(BAr^F_4)$ to form halide-abstracted $\mathbf{3}^+$ was notably not competent for reactions similar to those performed by $\mathbf{1}^+$ (i.e., H_2 activation and hydride abstraction). The acyl-containing $\mathbf{3}^+$ *does not* abstract a hydride from the substrate ^{Tol}ImH. We reason that this is due to an increased trans influence demonstrated by the acyl moiety in comparison with the carbamoyl moiety, emanating from π effects of the N lone-pair electrons of the carbamoyl group and as hinted by the MeCN-binding properties of the Pickett complex versus the Hu complex. We thus expected that the parent complex **3-Br** may exhibit the same reaction bias as observed for **2-PhCN** and attempted H_2 activation facilitated by exogenous base and hydride transfer experiments to organic substrates.

However, we surprisingly found that the introduction of one equiv of the exogenous base $[MeO^tBu_2ArO]^-$ resulted in deprotonation of a methylene proton of the acyl group in **3-Br** (Figure 7A), as initially evidenced by a noticeable color change from orange to red and a red shift in the IR frequencies of the $\nu(C{\equiv}O)$ features to 2021, 1998, 1962 and 1943 cm^{-1} (Table 1). Deprotonation was unambiguously confirmed by the molecular structure of **4-MeCN** (Figure 7B), revealing the generation of a C_2-symmetric dimer containing new and unexpected Fe−$C_{methine}$ bonds and thioether-S ligand displacement. The deprotonation event was readily reversible by addition of 2,6-lutidine·HBr to regenerate the starting compound **3-Br**. We initially suggested such reactivity of the methylene acyl moiety on the basis of ^{1}H NMR and IR spectroscopy[26] but only recently acquired unambiguous structural confirmation. We hypothesize that the acidic methylene protons are strongly related to the demonstrated instability of earlier model complexes containing acyl and thiolate ligands, which may result in methylene deprotonation and liberation of a protonated thiol ligand at temperatures above −40 °C.

We envisioned that **4-MeCN** might react with H_2, as the deprotonation of a methylene proton recalls the basic site resulting from dearomatization of methylene-linked PNP pincer ligand systems[54] (conventional organometallic catalysts) that facilitate H_2 activation and generates a pendent base on the ligand framework, analogous to the [Fe]-hydrogenase active site. Upon incubation with 7 atm D_2 gas, **4-MeCN** was shown to activate D_2, as evidenced by new resonances in the ^{2}H NMR spectrum at 2.59 and −14.90 ppm, corresponding to deuteration of the free ligand and formation of $[DFe_3(CO)_{11}]^-$. These new resonances also indicated (*i*) extrusion of the Fe metal center to liberate free ligand and (*ii*) reduction of the Fe metal center from Fe(II) to Fe(0). A series of control experiments were performed to elucidate a possible mechanism for these processes; these suggested that reduction of the Fe center results from generation of an unstable Fe−H species upon H_2 activation by **4-MeCN**. The resulting reductive elimination and $Fe(CO)_x$ extrusion consequently indicate deinsertion of the methylene−acyl moiety and further liberation of the now-protonated ligand.

Importance of the Facial Scaffold Approach: Pincer *mer*-C,N,S is Nonfunctional

Our group has also applied more conventional nonscaffolded, tridentate *mer*-C,N,S chelating ligands in the development of [Fe]-hydrogenase synthetic model compounds. We synthesized **5-Br** (Figure 4), the meridionally chelated carbamoyl thioether complex that is analogous to the *fac*-C,N,S compound **1-Br**.[25] Interestingly, *mer*-C,N,S ligated **5-Br** does not demonstrate any reactivity under H_2/D_2 atmospheres. The halide-abstracted compound $\mathbf{5}^+$ also does not result in NH/ND exchange, indicative of H_2/D_2 activation, across the carbamoyl moiety as was observed for $\mathbf{1}^+$. Furthermore, $\mathbf{5}^+$ does not abstract a hydride from the model substrate ^{Tol}ImH. The contrast in the reactivities of *mer*- and *fac*-C,N,S ligation underscores the importance of the facial C,N,S triad in the facilitating H_2 activation in the mononuclear [Fe]-hydrogenase.

Herein we convey new DFT calculations in order to understand the contrasting reactivities of *fac*-$\mathbf{1}^+$ and *mer*-$\mathbf{5}^+$ with H_2. Both *fac*-$\mathbf{1}^+$ and *mer*-$\mathbf{5}^+$ feature a d_{z^2}-like metal-centered LUMO along the axis of the unoccupied coordination site—the putative site of H_2 coordination—as depicted in Figure 8A,B. Importantly, the open coordination site is trans to

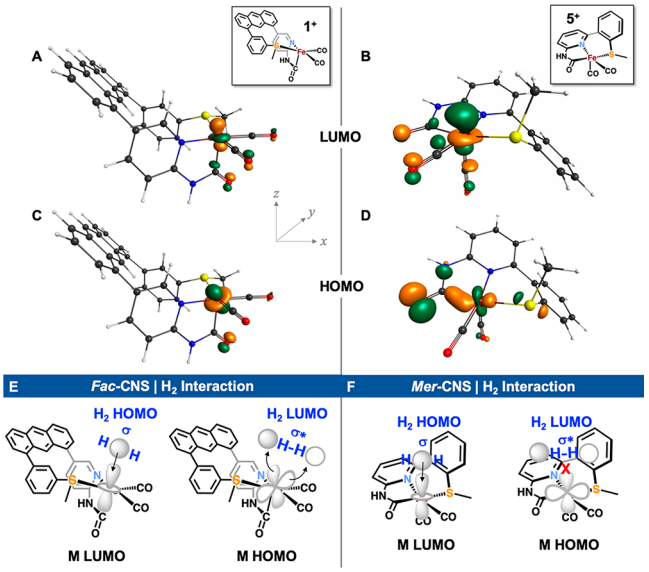

Figure 8. DFT (PW91/6-31G*)-calculated Kohn−Sham molecular orbital depictions of the LUMOs of (A) *fac*-$\mathbf{1}^+$ and (B) *mer*-$\mathbf{5}^+$ and HOMOs of (C) *fac*-$\mathbf{1}^+$ and (D) *mer*-$\mathbf{5}^+$. Proposed Kubas-type interactions of (E) *fac*-$\mathbf{1}^+$ with H_2 and (F) *mer*-$\mathbf{5}^+$ with H_2.

either the strongly σ-donating organometallic Fe−C bond in functional $\mathbf{1}^+$ or the π-accepting Fe-C≡O unit in nonfunctional $\mathbf{5}^+$. This is critical for the classical Kubas-type M−H_2 interaction, wherein electron density from the H−H σ bond is donated to an unoccupied metal orbital—ideally the d_{z^2} orbital as in these cases.[55−57]

However, the HOMOs of *fac*-$\mathbf{1}^+$ (Figure 8C) and *mer*-$\mathbf{5}^+$ (Figure 8D) differ substantially. The HOMO of *fac*-$\mathbf{1}^+$ is clearly a metal-centered nonbonding d_{xz} or d_{yz} orbital, ideally positioned at 45° with respect to the metal-centered LUMO and thus properly aligned for π donation into the σ^* orbital of H_2 in a classical Kubas-type interaction (Figure 8E). This results in a weakened H_2 bond and enables the experimentally observed NH/ND exchange processes upon incubation with H_2 gas. In contrast, the HOMO of *mer*-$\mathbf{5}^+$ is composed of the organometallic Fe−C σ bond and is coaligned (nonideally) with the *mer*-$\mathbf{5}^+$ LUMO. As a result, there is no favorable orbital alignment between the Fe $d_{xz}|d_{yz}$ and H_2 σ^* orbitals to

https://dx.doi.org/10.1021/acs.accounts.0c00315
Acc. Chem. Res. 2020, 53, 1637−1647

participate in a Kubas-type interaction (Figure 8F), which is required to activate H_2 and enable NH/ND exchange.

Complex **5-Br** was additionally used to investigate the viability of an Fe−H species in [Fe]-hydrogenase. Upon treatment of **5-Br** with the hydride donor $NaHBEt_3$ at −70 °C, an Fe−H resonance was observed at −5.08 ppm in the ^1H NMR spectrum.[24] However, the Fe−H species **5-H** decomposed at temperatures above −40 °C, resulting in extrusion of methylthiol and structural rearrangement to form a μ_2-methyl thiolate-bridged dimer. This observation suggests the feasibility of a transient Fe−H species supported by the primary coordination sphere of [Fe]-hydrogenase containing the organometallic Fe−C bond motif. Notably, the proposed hydride species **5-H** positions the hydride trans to a carbonyl ligand instead of the organometallic Fe−C bond, which should significantly influence the reactivity of the Fe−H moiety.

EXTANT CHALLENGES IN [FE]-HYDROGENASE SYNTHETIC MODELING

Several significant synthetic challenges and unanswered questions still remain to fully leverage the utility of synthetic modeling—and scaffolded ligands in particular—in understanding the chemistry performed by [Fe]-hydrogenase. To date, no direct evidence of intermediates relevant to [Fe]-hydrogenase catalysis have been observed in the biological system, and although mechanistic understanding has benefited from mutagenesis studies, it still largely relies on computation. Our group has now demonstrated the viability of C,N,S-supported Fe−H species relevant to proposed intermediates in [Fe]-hydrogenase catalysis. Still, such species are derived from thioether-ligated iron centers and thus result in the generation of formally neutral Fe−H species—in contrast to the likely formally anionic species encountered in nature. At present, we have been unable to detect the putative anionic Fe−H species in our thiolate-containing system **2-PhCN**, despite the fact that hydride transfer was observed. It may be the case that the strongly trans-influencing σ interaction of the organometallic Fe−C bond of the acyl moiety makes such an intermediate especially difficult to observe in comparison with the analogous trans-influencing but π-acidic CO ligand present in [FeFe]-hydrogenase. Thus, it may be necessary to incorporate further stabilizing moieties in the proximity of the Fe−H species, such as Lewis acidic centers or H-bond donors, to observe and characterize such an intermediate, as has been suggested by computation and structural biology. Isolation of such proposed synthetic intermediates would provide important spectroscopic standards for the hydride-bound state of [Fe]-hydrogenase to inform our understanding of the biologically unprecedented Fe−C acyl motif in controlling metal hydride reactivity. Contrastingly, perhaps the conformationally gated catalysis, highly preorganized enzyme−substrate complex, and unique organometallic Fe−C bond truly preclude a relevant Fe−H intermediate that is characteristic of other hydrogenases.

Relatedly, our studies utilizing both thiolato-S and thioether-S donors and their role in mediating hydride transfer or hydride abstraction, respectively, piqued our interest in the influence of the metal complex charge in mediating reactivity. In nature, the His14 residue is proposed to deprotonate the resting protonated 2-pyridinol moiety of the FeGP cofactor to enable heterolysis, acting as an important proton relay that additionally governs the charge and electron density at the Fe metal center. Furthermore, [Fe]-hydrogenase exhibits a functional preference/bias for H_2 generation at pH 6.5 (partial His protonation) and H_2 activation and hydride transfer at pH 7.5,[2] likely associated with His protonation/deprotonation and its importance in modulating the thermodynamic landscape of enzyme activity. Thus, we are interested in how incorporation of the 2-pyridinol moiety or other proton/charge-responsive moieties in our model systems will possibly enable bidirectional reactivity (Figure 9) characteristic of enzymatic systems.

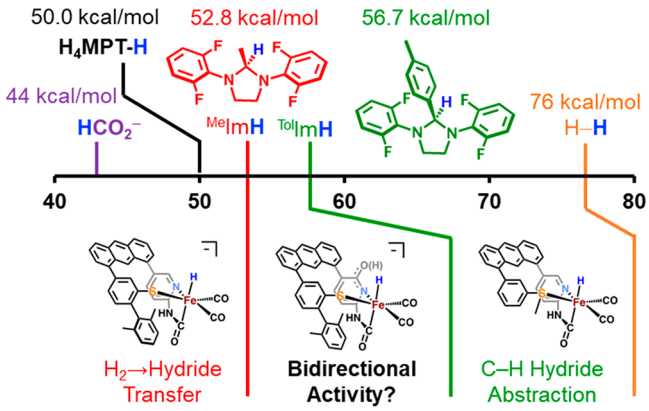

Figure 9. DFT-calculated substrate hydricities (in MeCN) and the corresponding scaffold model complexes that perform C−H hydride abstraction (from the substrate) or hydride transfer (to the substrate); this serves to bracket the hydricities of the corresponding Fe−H species from each ligand set. We hypothesize that the incorporation of the proton-active pyridone unit will provide intermediate hydricity and provide "gating" to bidirectional reactivity.

Indeed, the construction of protein-like microenvironments incorporating amino acid side chains in the extended ligand framework or the incorporation of synthetic complexes in protein hosts have improved the kinetics, thermodynamics, and chemical robustness of electrocatalytic synthetic hydrogenases;[58−65] however, this concept and the extension to the nonredox [Fe]-hydrogenase are still unexplored at present.

Our studies with acyl-containing model complexes highlight the difficulties of working with methylene-linked systems. While our scaffold approach effectively stabilized the core $\{Fe(CO)_2\}^{2+}$ motif of the acyl-containing parent complex **3-Br**, undesirable reactivity (i.e., methylene deprotonation) with exogenous base was still observed. We and others have now demonstrated the propensity of this moiety to initiate ligand loss triggered by CO deinsertion and subsequent protonation in synthetic systems. It remains to be seen whether scaffolded ligands containing thiolato-S ligands (in contrast to the weakly coordinating thioether-S donor) can be leveraged to enforce a more constrained geometry and disfavor this process. Furthermore, the incorporation of the biomimetic pyridone moiety may also preclude the undesired protonation/deligation reactions observed by modulation of the pK_a of both the methylene unit and putative Fe−H species. More predictable control over the reactivity of the acyl moiety in solution is certainly necessary before more progress can be made in understanding this unique ligation in nature. However, at present our work has demonstrated that biomimetic functional reactivity can be obtained with carbamoyl-containing model complexes and suggests that this ligation motif may provide a more accessible way forward.

https://dx.doi.org/10.1021/acs.accounts.0c00315
Acc. Chem. Res. 2020, 53, 1637−1647

CONCLUSION

In this Account, we have described our recent contributions to synthetic modeling of [Fe]-hydrogenase and the biomimetic reactivity with H_2 and model substrates. Our work utilizes rational design to probe the structural features that enable a holistic understanding of the role of active site components in the generation of functional model compounds. We have largely applied tridentate C,N,S chelating ligands derived from meridional pincer-type ligands and, with more functional success, facially coordinating anthracene-scaffolded ligands. Our model compounds highlight the critical structural organization of the heteroatom *fac*-C,N,S donors for H_2 interaction, supporting the critical role of the iron center in H_2 activation. Furthermore, we have demonstrated that both the *mer*- and *fac*-C,N,S coordination motifs that include organometallic Fe−C ligation can support Fe−H species derived from either hydride donor sources or gas incubation, respectively. Our research has demonstrated the functional differences between the carbamoyl and acyl structural motifs commonly employed in synthetic modeling of [Fe]-hydrogenase through differing hydride abstraction reactivities from model substrates and the role of a thiolate ligand in encouraging biomimetic hydride transfer reactivity. These advancements in the development of functional model compounds enabled by our scaffold approach serve as important benchmarks toward our research program's larger goal of applying synthetic modeling to observe and understand reactive intermediates of [Fe]-hydrogenase.

ASSOCIATED CONTENT

Supporting Information

The Supporting Information is available free of charge at https://pubs.acs.org/doi/10.1021/acs.accounts.0c00315.

Coordinates of unpublished optimized structures used for DFT calculations presented herein (PDF)

AUTHOR INFORMATION

Corresponding Author

Michael J. Rose − *Department of Chemistry, The University of Texas at Austin, Austin, Texas 78712, United States;* orcid.org/0000-0002-6960-6639; Email: mrose@cm.utexas.edu

Author

Spencer A. Kerns − *Department of Chemistry, The University of Texas at Austin, Austin, Texas 78712, United States;* orcid.org/0000-0001-6936-8098

Complete contact information is available at: https://pubs.acs.org/10.1021/acs.accounts.0c00315

Author Contributions

The manuscript was written through contributions of both authors. Both authors approved the final version of the manuscript.

Funding

This work was funded by the Welch Foundation (F-1822) and the National Science Foundation (NSF CHE-1808311).

Notes

The authors declare no competing financial interest.

Biographies

Spencer A. Kerns received his B.A. in Chemistry and Spanish at Auburn University in 2014 and completed his Ph.D. in the Rose lab at the University of Texas at Austin in 2020. He is currently a postdoctoral researcher in the Borovik lab at the University of California, Irvine.

Michael J. Rose is an Associate Professor in the Chemistry Department at the University of Texas at Austin. He received his B.S. from the University of California, Davis, and his Ph.D. at the University of California, Santa Cruz, advised by Pradip K. Mascharak, after which he undertook postdoctoral training under Harry B. Gray and Nathan S. Lewis at California Institute of Technology (CCI Solar and NSF ACC-F Fellowships). His research includes synthetic bioinorganic chemistry of [Fe]-hydrogenase and nitrogenase as well as silicon-based solar fuels and heavy main-group chemistry.

ACKNOWLEDGMENTS

The authors gratefully acknowledge the work of Dr. Junhyeok Seo, Dr. Zhulin (Sam) Xie, and Dr. Taylor Manes for their contributions to the research presented in this Account. The authors also acknowledge Prof. Richard Jones for computational access to his licensed copy of Gaussian 16 used for DFT calculations on the organic substrates.

REFERENCES

(1) Schilter, D.; Camara, J. M.; Huynh, M. T.; Hammes-Schiffer, S.; Rauchfuss, T. B. Hydrogenase Enzymes and Their Synthetic Models: The Role of Metal Hydrides. *Chem. Rev.* **2016**, *116*, 8693−8749.

(2) Zirngibl, C.; Hedderich, R.; Thauer, R. K. N^5,N^{10}-Methylenetetrahydromethanopterin Dehydrogenase from *Methanobacterium thermoautotrophicum* Has Hydrogenase Activity. *FEBS Lett.* **1990**, *261*, 112−116.

(3) Shima, S.; Pilak, O.; Vogt, S.; Schick, M.; Stagni, M. S.; Meyer-Klaucke, W.; Warkentin, E.; Thauer, R. K.; Ermler, U. The Crystal Structure of [Fe]-Hydrogenase Reveals the Geometry of the Active Site. *Science* **2008**, *321*, 572−575.

(4) Hiromoto, T.; Ataka, K.; Pilak, O.; Vogt, S.; Stagni, M. S.; Meyer-Klaucke, W.; Warkentin, E.; Thauer, R. K.; Shima, S.; Ermler, U. The Crystal Structure of C176A Mutated [Fe]-Hydrogenase Suggests an Acyl−Iron Ligation in the Active Site Iron Complex. *FEBS Lett.* **2009**, *583*, 585−590.

(5) Vignais, P. M.; Billoud, B.; Meyer, J. Classification and Phylogeny of Hydrogenases. *FEMS Microbiol. Rev.* **2001**, *25*, 455−501.

(6) Tard, C.; Pickett, C. J. Structural and Functional Analogues of the Active Sites of the [Fe]-, [NiFe]-, and [FeFe]-Hydrogenases. *Chem. Rev.* **2009**, *109*, 2245−2274.

(7) Huang, G.; Wagner, T.; Wodrich, M. D.; Ataka, K.; Bill, E.; Ermler, U.; Hu, X.; Shima, S. The Atomic-Resolution Crystal Structure of Activated [Fe]-Hydrogenase. *Nat. Catal.* **2019**, *2*, 537−543.

(8) Obrist, B. V.; Chen, D.; Ahrens, A.; Schunemann, V.; Scopelliti, R.; Hu, X. An Iron Carbonyl Pyridonate Complex Related to the Active Site of the [Fe]-Hydrogenase (Hmd). *Inorg. Chem.* **2009**, *48*, 3514−3516.

(9) Chen, D.; Scopelliti, R.; Hu, X. [Fe]-Hydrogenase Models Featuring Acylmethylpyridinyl Ligands. *Angew. Chem., Int. Ed.* **2010**, *49*, 7512−7515.

(10) Chen, D.; Scopelliti, R.; Hu, X. A Five-Coordinate Iron Center in the Active Site of [Fe]-Hydrogenase: Hints from a Model Study. *Angew. Chem., Int. Ed.* **2011**, *50*, 5671−5673.

(11) Turrell, P. J.; Wright, J. A.; Peck, J. N. T.; Oganesyan, V. S.; Pickett, C. J. The Third Hydrogenase: A Ferracyclic Carbamoyl with Close Structural Analogy to the Active Site of Hmd. *Angew. Chem., Int. Ed.* **2010**, *49*, 7508−7511.

(12) Song, L.-C.; Xie, Z.-J.; Wang, M.-M.; Zhao, G.-Y.; Song, H.-B. Biomimetic Models for the Active Site of [Fe]Hydrogenase Featuring an Acylmethyl(hydroxymethyl)pyridine Ligand. *Inorg. Chem.* **2012**, *51*, 7466−7468.
(13) Song, L.-C.; Zhu, L.; Liu, B.-B. A Biomimetic Model for the Active Site of [Fe]-H_2ase Featuring a 2-Methoxy-3,5-dimethyl-4-phosphato-6-acylmethylpyridine Ligand. *Organometallics* **2019**, *38*, 4071−4075.
(14) Hu, B.; Chen, D.; Hu, X. Synthesis and Reactivity of Mononuclear Iron Models of [Fe]-Hydrogenase That Contain an Acylmethylpyridinol Ligand. *Chem. - Eur. J.* **2014**, *20*, 1677−1682.
(15) Song, L.-C.; Zhao, G.-Y.; Xie, Z.-J.; Zhang, J.-W. A Novel Acylmethylpyridinol Ligand Containing Dinuclear Iron Complex Closely Related to [Fe]-Hydrogenase. *Organometallics* **2013**, *32*, 2509−2512.
(16) Turrell, P. J.; Hill, A. D.; Ibrahim, S. K.; Wright, J. A.; Pickett, C. J. Ferracyclic Carbamoyl Complexes Related to the Active Site of [Fe]-Hydrogenase. *Dalton Trans.* **2013**, *42*, 8140−8146.
(17) Dey, A. Density Functional Theory Calculations on the Mononuclear Non-Heme Iron Active Site of Hmd Hydrogenase: Role of the Internal Ligands in Tuning External Ligand Binding and Driving H_2 Heterolysis. *J. Am. Chem. Soc.* **2010**, *132*, 13892−13901.
(18) Xu, T.; Yin, C.-J. M.; Wodrich, M. D.; Mazza, S.; Schultz, K. M.; Scopelliti, R.; Hu, X. A Functional Model of [Fe]-Hydrogenase. *J. Am. Chem. Soc.* **2016**, *138*, 3270−3273.
(19) Shima, S.; Chen, D.; Xu, T.; Wodrich, M. D.; Fujishiro, T.; Schultz, K. M.; Kahnt, J.; Ataka, K.; Hu, X. Reconstitution of [Fe]-Hydrogenase Using Model Complexes. *Nat. Chem.* **2015**, *7*, 995−1002.
(20) Seo, J.; Ali, A. K.; Rose, M. J. Novel Ligand Architectures for Metalloenzyme Modeling: Anthracene-Based Ligands for Synthetic Modeling of Mono-[Fe] Hydrogenase. *Comments Inorg. Chem.* **2014**, *34*, 103−113.
(21) Seo, J.; Manes, T. A.; Rose, M. J. Structural and Functional Synthetic Model of Mono-Iron Hydrogenase Featuring an Anthracene Scaffold. *Nat. Chem.* **2017**, *9*, 552−557.
(22) Kerns, S. A.; Magtaan, A.-C.; Vong, P. R.; Rose, M. J. Functional Hydride Transfer by a Thiolate-Containing Model of Mono-Iron Hydrogenase Featuring an Anthracene Scaffold. *Angew. Chem., Int. Ed.* **2018**, *57*, 2855−2858.
(23) Kerns, S. A.; Seo, J.; Lynch, V. M.; Shearer, J.; Sullivan, E. R.; Rose, M. J. Scaffold-Based [Fe]-Hydrogenase Iron−Acyl Model: Functional H_2 Activation Contrasts with Off-Pathway Hydride-Induced $Iron^0$ (Carbonyl) Extrusion.
(24) Durgaprasad, G.; Xie, Z.-L.; Rose, M. J. Iron Hydride Detection and Intramolecular Hydride Transfer in a Synthetic Model of Mono-Iron Hydrogenase with a CNS Chelate. *Inorg. Chem.* **2016**, *55*, 386−389.
(25) Xie, Z.-L.; Durgaprasad, G.; Ali, A. K.; Rose, M. J. Substitution Reactions of Iron(II) Carbamoyl−Thioether Complexes Related to Mono-Iron Hydrogenase. *Dalton Trans.* **2017**, *46*, 10814−10829.
(26) Cho, Y.; Durgaprasad, G.; Rose, M. J. CNS and CNP Iron(II) Mono-Iron Hydrogenase (Hmd) Mimics: Role of Deprotonated Methylene(Acyl) and the Trans-Acyl Site in H_2 Heterolysis. *Inorg. Chem.* **2019**, *58*, 12689−12699.
(27) Muthiah, K. A. T.; Durgaprasad, G.; Xie, Z.-L.; Williams, O. M.; Joseph, C.; Lynch, V. M.; Rose, M. J. Mononuclear Iron(II) Dicarbonyls Derived from NNS Ligands—Structural Models Related to a "Pre-Acyl" Active Site of Mono-Iron (Hmd) Hydrogenase. *Eur. J. Inorg. Chem.* **2015**, *2015*, 1675−1691.
(28) Xie, Z.-L.; Pennington, D. L.; Boucher, D. G.; Lo, J.; Rose, M. J. Effects of Thiolate Ligation in Monoiron Hydrogenase (Hmd): Stability of the $\{Fe(CO)_2\}^{2+}$ Core with NNS Ligands. *Inorg. Chem.* **2018**, *57*, 10028−10039.
(29) Yang, X.; Hall, M. B. Trigger Mechanism for the Catalytic Hydrogen Activation by Monoiron (Iron-Sulfur Cluster-Free) Hydrogenase. *J. Am. Chem. Soc.* **2008**, *130*, 14036−14037.
(30) Yang, X.; Hall, M. B. Monoiron Hydrogenase Catalysis: Hydrogen Activation with the Formation of a Dihydrogen, $Fe{-}H^{\delta-}\cdots H^{\delta+}{-}O$, Bond and Methenyl-$H_4MPT^+$ Triggered Hydride Transfer. *J. Am. Chem. Soc.* **2009**, *131*, 10901−10908.
(31) Klein, A. R.; Hartmann, G. C.; Thauer, R. K. Hydrogen Isotope Effects in the Reactions Catalyzed by H_2-Forming N^5,N^{10}-Methylenetetrahydromethanopterin Dehydrogenase from Methanogenic Archaea. *Eur. J. Biochem.* **1995**, *233*, 372−376.
(32) Finkelmann, A. R.; Senn, H. M.; Reiher, M. Hydrogen-Activation Mechanism of [Fe] Hydrogenase Revealed by Multi-Scale Modeling. *Chem. Sci.* **2014**, *5*, 4474−4482.
(33) Shima, S.; Lyon, E. J.; Thauer, R. K.; Mienert, B.; Bill, E. Mossbauer Studies of the Iron-Sulfur Cluster-Free Hydrogenase: The Electronic State of the Mononuclear Fe Active Site. *J. Am. Chem. Soc.* **2005**, *127*, 10430−10435.
(34) Gubler, J.; Finkelmann, A. R.; Reiher, M. Theoretical ^{57}Fe Mössbauer Spectroscopy for Structure Elucidation of [Fe] Hydrogenase Active Site Intermediates. *Inorg. Chem.* **2013**, *52*, 14205−14215.
(35) Fischer, A. A.; Lindeman, S. V.; Fiedler, A. T. A Synthetic Model of the Nonheme Iron−Superoxo Intermediate of Cysteine Dioxygenase. *Chem. Commun.* **2018**, *54*, 11344−11347.
(36) Park, D.; Lee, M. S. Kinetic Study of Catalytic CO_2 Hydration by Metal-Substituted Biomimetic Carbonic Anhydrase Model Complexes. *R. Soc. Open Sci.* **2019**, *6*, 190407−190415.
(37) Zhou, J.; Hu, Z.; Münck, E.; Holm, R. H. The Cuboidal Fe_3S_4 Cluster: Synthesis, Stability, and Geometric and Electronic Structures in a Non-Protein Environment. *J. Am. Chem. Soc.* **1996**, *118*, 1966−1980.
(38) Kanady, J. S.; Tsui, E. Y.; Day, M. W.; Agapie, T. A Synthetic Model of the Mn_3Ca Subsite of the Oxygen-Evolving Complex in Photosystem II. *Science* **2011**, *333*, 733−736.
(39) Ye, M.; Thompson, N. B.; Brown, A. C.; Suess, D. L. M. A Synthetic Model of Enzymatic $[Fe_4S_4]$−Alkyl Intermediates. *J. Am. Chem. Soc.* **2019**, *141*, 13330−13335.
(40) Li, Y.; Cao, R.; Lippard, S. J. Design and Synthesis of a Novel Triptycene-Based Ligand for Modeling Carboxylate-Bridged Diiron Enzyme Active Sites. *Org. Lett.* **2011**, *13*, 5052−5055.
(41) Ding, K.; Miller, D. L.; Young, V. G.; Lu, C. C. Study of the Conformationally Flexible, Wide Bite-Angle Diphosphine 4,6-Bis(3-diisopropylphosphinophenyl)dibenzofuran in Rhodium(I) and Palladium(II) Coordination Complexes. *Inorg. Chem.* **2011**, *50*, 2545−2552.
(42) Marlier, E. E.; Tereniak, S. J.; Ding, K.; Mulliken, J. E.; Lu, C. C. First-Row Transition-Metal Chloride Complexes of the Wide Bite-Angle Diphosphine IPrDPDBFphos and Reactivity Studies of Monovalent Nickel. *Inorg. Chem.* **2011**, *50*, 9290−9299.
(43) Kaganovsky, L.; Cho, K.-B.; Gelman, D. New Trans-Chelating Ligands and Their Complexes and Catalytic Properties in the Mizoroki−Heck Arylation of Cyclohexene. *Organometallics* **2008**, *27*, 5139−5145.
(44) Kaganovsky, L.; Gelman, D.; Rueck-Braun, K. Trans-Chelating Ligands in Palladium-Catalyzed Carbonylative Coupling and Methoxycarbonylation of Aryl Halides. *J. Organomet. Chem.* **2010**, *695*, 260−266.
(45) Manes, T. A.; Rose, M. J. Rigid Scaffolds for the Design of Molecular Catalysts and Biomimetic Active Sites: A Case Study of Anthracene-Based Ligands for Modeling Mono-Iron Hydrogenase (Hmd). *Coord. Chem. Rev.* **2017**, *353*, 295−308.
(46) Kalz, K. F.; Brinkmeier, A.; Dechert, S.; Mata, R. A.; Meyer, F. Functional Model for the [Fe] Hydrogenase Inspired by the Frustrated Lewis Pair Concept. *J. Am. Chem. Soc.* **2014**, *136*, 16626−16634.
(47) Ilic, S.; Pandey Kadel, U.; Basdogan, Y.; Keith, J. A.; Glusac, K. D. Thermodynamic Hydricities of Biomimetic Organic Hydride Donors. *J. Am. Chem. Soc.* **2018**, *140*, 4569−4579.
(48) Heiden, Z. M.; Lathem, A. P. Establishing the Hydride Donor Abilities of Main Group Hydrides. *Organometallics* **2015**, *34*, 1818−1827.

https://dx.doi.org/10.1021/acs.accounts.0c00315
Acc. Chem. Res. 2020, 53, 1637−1647

(49) Cohen, L. A.; Jones, W. M. A Study of Free Energy Relationships in Hindered Phenols. Correlation of Spectral Properties with Substituent Constants. *J. Am. Chem. Soc.* **1963**, *85*, 3402−3406.
(50) Zhang, X.-M.; Bordwell, F. G. Element Effects on the Homolytic Bond Dissociation Enthalpies of the Acidic H−A Bonds in $HA^{\bullet+}$ Radical Cations and Their Neutral Precursors. *J. Am. Chem. Soc.* **1994**, *116*, 4251−4254.
(51) Bunting, J. W.; Toth, A.; Heo, C. K. M.; Moors, R. G. Equilibration of *N*-(2-Cyanoethyl)pyridinium Cations with Substituted Pyridines and Acrylonitrile. A Change in Rate-Determining Step in an E1cb Reaction. *J. Am. Chem. Soc.* **1990**, *112*, 8878−8885.
(52) Lyon, E. J.; Shima, S.; Boecher, R.; Thauer, R. K.; Grevels, F.-W.; Bill, E.; Roseboom, W.; Albracht, S. P. J. Carbon Monoxide as an Intrinsic Ligand to Iron in the Active Site of the Iron-Sulfur-Cluster-Free Hydrogenase H_2-Forming Methylenetetrahydromethanopterin Dehydrogenase As Revealed by Infrared Spectroscopy. *J. Am. Chem. Soc.* **2004**, *126*, 14239−14248.
(53) Shima, S.; Schick, M.; Kahnt, J.; Ataka, K.; Steinbach, K.; Linne, U. Evidence for Acyl−Iron Ligation in the Active Site of [Fe]-Hydrogenase Provided by Mass Spectrometry and Infrared Spectroscopy. *Dalt. Trans.* **2012**, *41*, 767−771.
(54) Gunanathan, C.; Milstein, D. Metal−Ligand Cooperation by Aromatization−Dearomatization: A New Paradigm in Bond Activation and "Green" Catalysis. *Acc. Chem. Res.* **2011**, *44*, 588−602.
(55) Kubas, G. J. Fundamentals of H_2 Binding and Reactivity on Transition Metals Underlying Hydrogenase Function and H_2 Production and Storage. *Chem. Rev.* **2007**, *107*, 4152−4205.
(56) Kubas, G. J. Metal−Dihydrogen and σ-Bond Coordination: The Consummate Extension of the Dewar−Chatt−Duncanson Model for Metal−Olefin π Bonding. *J. Organomet. Chem.* **2001**, *635*, 37−68.
(57) Gordon, J. C.; Kubas, G. J. Perspectives on How Nature Employs the Principles of Organometallic Chemistry in Dihydrogen Activation in Hydrogenases. *Organometallics* **2010**, *29*, 4682−4701.
(58) Priyadarshani, N.; Dutta, A.; Ginovska, B.; Buchko, G. W.; O'Hagan, M.; Raugei, S.; Shaw, W. J. Achieving Reversible H_2/H^+ Interconversion at Room Temperature with Enzyme-Inspired Molecular Complexes: A Mechanistic Study. *ACS Catal.* **2016**, *6*, 6037−6049.
(59) Boralugodage, N. P.; Arachchige, R. J.; Dutta, A.; Buchko, G. W.; Shaw, W. J. Evaluating the Role of Acidic, Basic, and Polar Amino Acids and Dipeptides on a Molecular Electrocatalyst for H_2 Oxidation. *Catal. Sci. Technol.* **2017**, *7*, 1108−1121.
(60) Kandemir, B.; Kubie, L.; Guo, Y.; Sheldon, B.; Bren, K. L. Hydrogen Evolution from Water under Aerobic Conditions Catalyzed by a Cobalt ATCUN Metallopeptide. *Inorg. Chem.* **2016**, *55*, 1355−1357.
(61) Chakraborty, S.; Edwards, E. H.; Kandemir, B.; Bren, K. L. Photochemical Hydrogen Evolution from Neutral Water with a Cobalt Metallopeptide Catalyst. *Inorg. Chem.* **2019**, *58*, 16402−16410.
(62) Dutta, A.; Hamilton, G. A.; Hartnett, H. E.; Jones, A. K. Construction of Heterometallic Clusters in a Small Peptide Scaffold as [NiFe]-Hydrogenase Models: Development of a Synthetic Methodology. *Inorg. Chem.* **2012**, *51*, 9580−9588.
(63) Roy, S.; Nguyen, T.-A. D.; Gan, L.; Jones, A. K. Biomimetic Peptide-Based Models of [FeFe]-Hydrogenases: Utilization of Phosphine-Containing Peptides. *Dalton Trans.* **2015**, *44*, 14865−14876.
(64) Call, A.; Casadevall, C.; Romero-Rivera, A.; Martin-Diaconescu, V.; Sommer, D. J.; Osuna, S.; Ghirlanda, G.; Lloret-Fillol, J. Improved Electro- and Photocatalytic Water Reduction by Confined Cobalt Catalysts in Streptavidin. *ACS Catal.* **2019**, *9*, 5837−5846.
(65) Bacchi, M.; Veinberg, E.; Field, M. J.; Niklas, J.; Matsui, T.; Tiede, D. M.; Poluektov, O. G.; Ikeda-Saito, M.; Fontecave, M.; Artero, V. Artificial Hydrogenases Based on Cobaloximes and Heme Oxygenase. *ChemPlusChem* **2016**, *81*, 1083−1089.

https://dx.doi.org/10.1021/acs.accounts.0c00315
Acc. Chem. Res. 2020, 53, 1637−1647